Journal of Constructional Steel Research 117 (2016) 115–125

Contents lists available at ScienceDirect

Journal of Constructional Steel Research

Numerical and experimental evaluation of a developed nonlinear curved spring element under compression force

Amir Fateh, Farzad Hejazi *, Mohd Saleh Jaafar, Izian Abd Karim

Department of Civil Engineering, Faculty of Engineering, University Putra Malaysia, Serdang, Selangor, Darul Ehsan, 43400, Malaysia

ARTICLE INFO

Article history:
Received 20 March 2015
Received in revised form 2 October 2015
Accepted 17 October 2015
Available online 24 October 2015

Keywords:
Variable stiffness bracing system
Finite element simulation
Mathematical model
Energy dissipation system
Direct compression test

ABSTRACT

This paper presents an evaluation of a curved spring element that may be utilized in a developed variable stiffness bracing (VSB) system to confer the variable stiffness characteristic of the system.VSB system is established to protect the structure against dynamic loads induced by earthquake, wind and etc. To obtain the curved shape of the spring, mathematical modeling is conducted. Direct compression experimental tests are conducted for a variety of models with different thicknesses and materials. The results of the experiments show a nonlinear stiffness trend for the curved spring element. In addition, to observe the yielding of the curved spring, different strain gauges are installed in several positions to record the strain in the models during the application of compression load. The results reveal that the geometry and material characteristics have an important effect on the stiffness value of the spring. Furthermore, finite element simulations of models are performed, and results are compared with those of experimental tests. The results from the experiments, as well as model and finite element simulation, show the curved spring's potential to be used in the developed VSB system and can be installed as a lateral resistance system in a structure subjected to vibration excitation such as an earthquake. Finally, the efficiency of the aforementioned system is evaluated via pushover analysis in a bare frame via finite element simulation. The results from pushover analysis illustrate the efficiency of the variable stiffness bracing system in framed structures.

1. Introduction

Diminishing the vibration effects in structures subjected to dynamic loads, such as earthquake, wind, and so on, attract enormous attention among structural engineers, experts, and researchers. Seismic vibration, in particular, can induce unnecessary oscillations to buildings, and these oscillations may cause catastrophic failure of structural components. In the last two decades, much research has been done to improve the lateral resistance of structural systems. In addition, a few vibration control techniques have been proposed to achieve a more economical and safer structural design [1]. Conventional seismic design philosophy has relied on the dissipation of input seismic energy through the inherent ductility of structural sections during large strains in the main elements. Employing supplemental energy dissipation devices that are not associated with the main lateral resisting system have been developed and designed specifically as external devices to dissipate seismic energy because the conventional approach may lead to unrealistic and uneconomical design as well as structural damage. These devices can be easily substituted after severe excitation [2,3]. Control methods used in design practices can be generally categorized into three types: active control [4], passive control, and semi-active control [5].

Desired effects of active variable stiffness (AVS) systems on structural seismic performance have been proven in previous studies [6–8]. Such techniques have been investigated experimentally and implemented on a full-scale building in Japan [9,10]. However, most available variable stiffness systems are operated using an external electrical controller that might cause a lag in efficient performance. These systems highly depend on an energy resource and also require repetitive maintenance. Therefore, developing a real-time system that does not rely on an energy resource and maintenance process is imperative. A non-resonant control method has been implemented in a variable stiffness device in a previous research [11]. Furthermore, the performance of a new design of variable stiffness mount with pre-stress stiffness of a cable-based mechanism has been experimentally proven [12]. Another type of variable stiffness actuator that included an electrical DC motor and an elastic device (as main mechanical structure of system) has been proposed to be adapted with dynamic external forces. [13]. Moreover, optimization of active variable stiffness action in multi-degree structure has been conducted through a computational algorithm [14,15].

Due to more complexity of structural systems and the higher seismic motion required higher operation energy is required to perform force-type systems. A port-based mathematical outline for modeling and

* Corresponding author.
E-mail addresses: amirfateh.saze@yahoo.com (A. Fateh), farzad@fhejazi.com (F. Hejazi), msj@upm.my (M.S. Jaafar), izian_abd@upm.edu.my (I.A. Karim).

http://dx.doi.org/10.1016/j.jcsr.2015.10.011

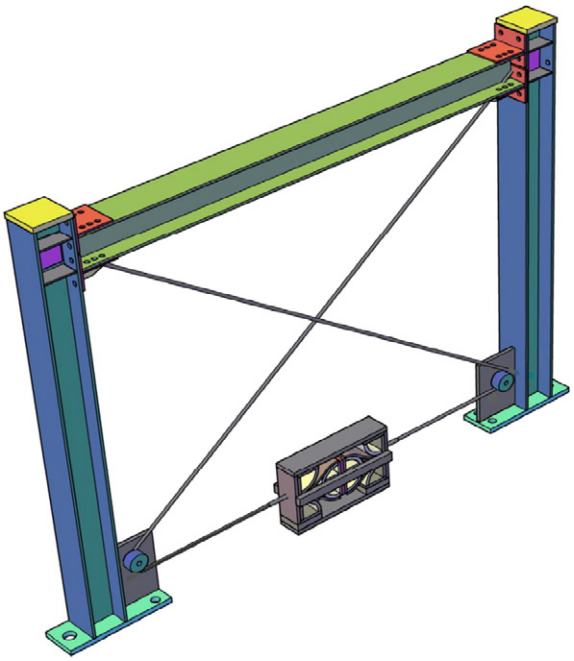

Fig. 1. Installation layout of VSB system on a frame. (a) Imposed cyclic load (b) left to right action (c) right to left action.

evaluating of variable stiffness actuators has been provided as an essential energy efficient design framework of variable stiffness actuators [16]. Besides, in order to dominate the energy issues, numerous semi-active and hybrid method have been introduced [17–19]. Additionally, approximate mode superposition (AMS) has been proposed as a technique for seismic design of structures furnished by active variable stiffness systems [20].

A variable-stiffness isolation method, where isolation stiffness can be changed instantly in response to the earthquake was presented by previous researches in different aspects [21–24]. For example, Leverage-type stiffness controllable isolation system (LSCIS) has been developed as a system which has been able to offer better seismic performance compared to conventional isolation with unchangeable stiffness [25].

In high-seismicity regions, moment-resisting steel frames (MRSF) are regularly chosen because of their sufficient energy dissipation capacity, which is reflected by the large plastic deformation of elements in the moment resistance frames [26]. This ability allows structural engineers to design mentioned frames under the minimum lateral force compared with other structural systems. On the other hand, unanticipated severe incidence may result in an unacceptable large story drift. Recent earthquake events have highlighted the unavoidability of seismic retrofitting of the presented moment frames. Furthermore, retrofit design by using braces as retrofitting components must include meticulous consideration of the brace addition effects on the original frames.

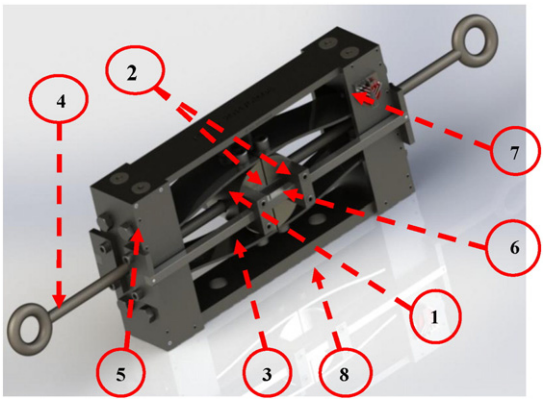

Fig. 3. Schematic view of the developed VSB system (PI NO:2,014,701,608).

Numerical analysis of variable stiffness bracing system (VSB) implementation in frame structure discussed and results shows the efficiency of system to reduce the seismic effects [27].

In this study, the new bracing system with nonlinear leaf spring developed as adaptive structural control system to protect the building against severe vibration and ground movement. The VSB device includes two nonlinear leaf springs in each side which provide nonlinear stiffness at different displacement of frame. Application of VSB device in framed building does not scarify the inherent energy dissipation characteristics and ductility capability of moment resisting frame. For large vibration amplitudes, the bracing member and nonlinear spring acting and restrain unacceptable story drift. This device can be considered as an alternative to rapid retrofitting system for MSRF building.

Since the VSB is developed in this study, mathematical model, experimental and finite element simulation must be conducted in order to assess the spring performance. By other words, the current study attempted to formulate the spring shape profile and evaluated the spring action based on experiments and finite element simulation. Experimental models and finite element's model considered as same geometry and material specification in order to compare and verify the obtained results.

2. Development of a VSB system

Fig. 1 demonstrates the installation layout of the VSB system on a frame. The VSB system is fastened to a frame with wire cables. The base plate of the VSB system is connected by bolts to either the lower beam or foundation depending on the installation's location. The wire ropes are joined to the rods in the VSB system. The VSB device is subjected to lateral load. Whenever the frame is subjected to vibration, the VSB system moves back and forth. The cables operate as the buckling-free member and transfer the tensile force to the VSB system and induce compression force in the curved springs; thus, the proposed system can control the story displacement within the particular limitation. This study attempts to design an effective approach to control structural

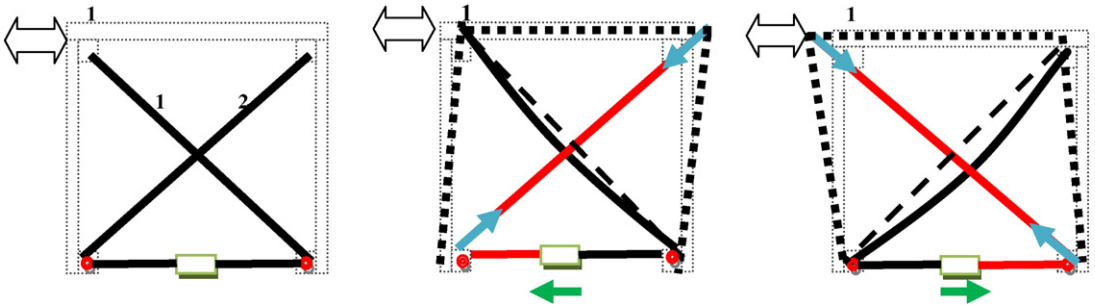

Fig. 2. Action of VSB System in frame.

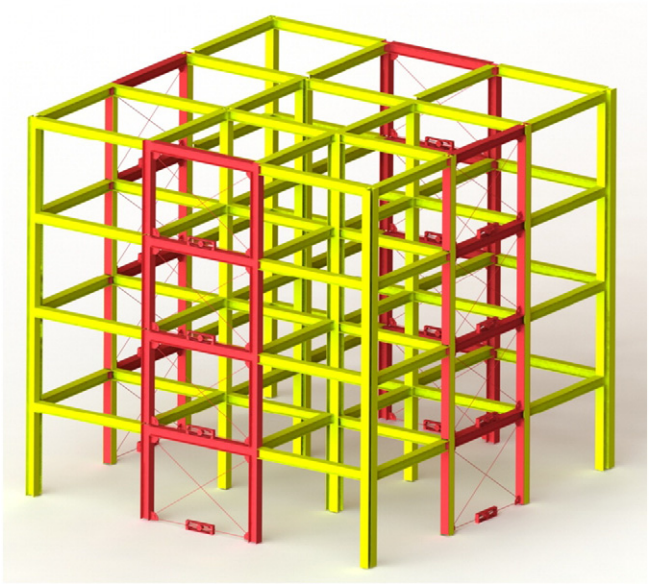

Fig. 4. 3D view of the VSB installation in framed building. (a) Installation of VSB device at foundation. (b) Installation of VSB device at story level.

response to vibration. The design procedure of the VSB system is optimized through different aspects to increase system functionality and reduce vibration effects in structures.

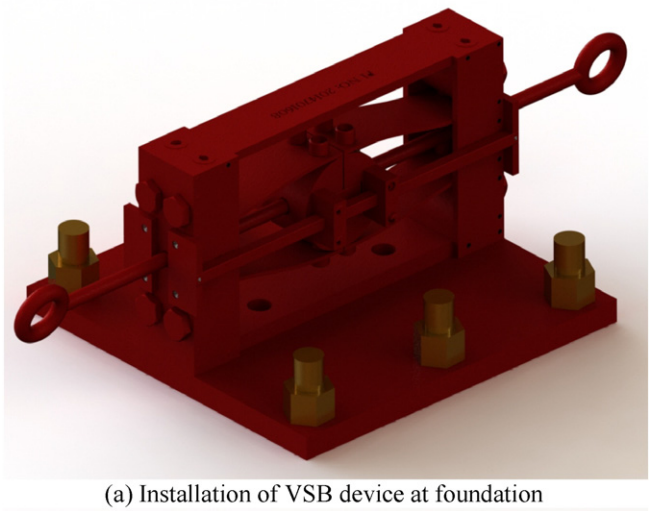

(a) Installation of VSB device at foundation

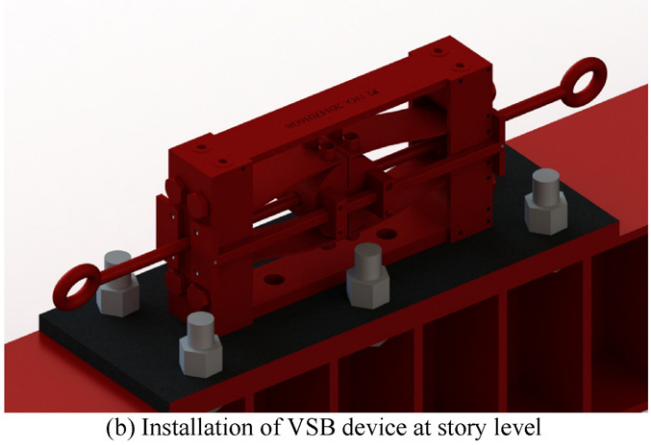

(b) Installation of VSB device at story level

Fig. 5. Installation of VSB device at different location.

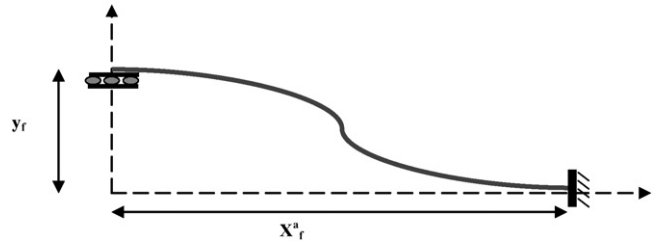

Fig. 6. Structural model of curved leaf spring.

The device action subjected to the vibration load is depicted in Fig. 2. Assume that the lateral load is imposed at the top of the frame (Node 1) from left to right and side versa. The frame is intended to move to the right and sides. In the case of left to right movement, Cable 1 is operated as the compression member and will be buckled [Fig. 2(b)]. Nevertheless, the buckling deficiency of component because of compression load is abolished completely due to the employ of cables. By contrast, Cable 2 acts as a tension member, and corresponding tensile force is transferred to the device. Therefore the VSB is desired to move to the left side. Moreover in the case of right to left movement, Cables 1 and 2 are operated as compression and tension elements, respectively [Fig. 2(c)]. In this situation, the VSB device tends to shift to the right side but in both directions of movement the leaf springs resist against the transferred forces from cables in to the device.

Fig. 3 demonstrates the schematic view of the VSB system. Four curved springs operate in bending conditions under a large displacement (Label 1). Label 2 refers to a cylindrical solid element that can shift back and forth in a longitudinal direction (one-dimensional direction) along with steel rails on both sides (Label 3). The steel rods (Label 4) are passed through each side's plates (Label 5) and fixed to the cubic core (Label 6). Whenever force is transferred from the cable, the steel cubic core moves and comes in contact with the C-shaped cylindrical solid member (Label 2), where the spring is fixed. The C-shaped elements help maintain the initial shape of the curved spring during system performance. In the other words, the global stiffness of the nonlinear spring must be protected from curvature extension. Therefore, four quarter solid cylinders (Label

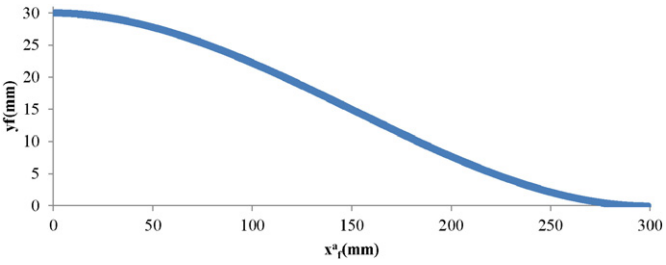

Fig. 7. Shape of the curved spring for the experimental model.

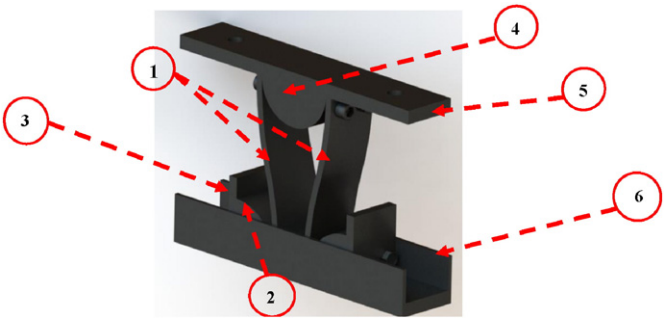

Fig. 8. Schematic view of half VSB model for direct compression test.

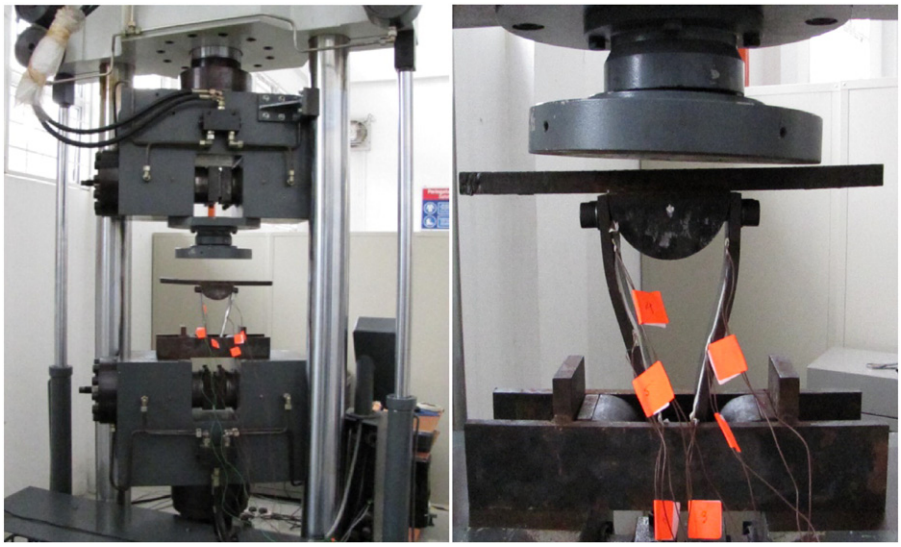

Fig. 9. Direct compression test setup (PI NO: 2,014,701,608).

7) and two C-shaped (Label 2) elements are essential to function as supports. As previously pointed out, this system increases the lateral stiffness of a story without reducing the impact on the moment's frame ductility. The VSB bracing system was not designed for small or medium vibration amplitudes; it is especially made for large ones and even controls unacceptably large story drift. The VSB system can easily be installed on the bottom beam or foundation by the aid of a horizontal VSB plate (Label 8). Fig. 4 shows the suggested locations of VSB device in 4 story framed building. This installation layout may be changed due to architectural and design constraints. Whereas the VSB action is considered for in-plane movement, it must be installed in both directions of frame building to capture the seismic loads transferred to major axes of structures such as available lateral resistant systems. For installation of VSB, the proper bays must be chosen without any limitation in terms of architectural concerns and possibility of device connections either to beam or foundation. Moreover this device can be installed instead of other conventional lateral resisting system such as infill wall and bracing element. Furthermore the closed view of VSB device installation at foundation and story level is presented in Fig. 5.

3. Mathematical model

As shown in Fig. 6, leaf spring can be considered as curved beam structure fixed at one side and fixed roller at another extreme which is acting just in bending situation under large displacements. In this case the normal beam curvature equation cannot be generally linearized. Therefore the following assumption is applied. For a fixed roller point specified by the aspect ratio $\alpha = x^a_f/y_f$, the deformed shape $y(x)$ for the leaf spring in Fig. 7 can be derived by solving the nonlinear differential equation (Eq. (1)) [28]. x^a_f and y_f show the horizontal and vertical distances of the leaf spring, respectively. The boundary conditions in the structural model of the curved leaf spring are as follow:

$$y(0) = y_f; y'(0) = 0; y\left(x_f^{\alpha}\right) = 0; y'\left(x_f^{\alpha}\right) = 0$$
$$\frac{d^2}{dx^2}\left(\mathrm{EI}\frac{y''(x)}{\left(1+y'(x)^2\right)^{3/2}}\right) = 0, \quad (1)$$
$$0 < x < x_f^a$$

where EI, $y'(x)$ and $y''(x)$ are flexural stiffness, first and second derivation of profile deformation shape respectively.

The boundary conditions at the left fixed roller support (x = 0) shows that the spring is clamped at the indicated points. In addition, at the lower extreme (roller support $x = x^{\alpha}_f$), the spring is clamped but can move in a longitudinal direction. However, such a differential equation is exceedingly nonlinear. For this specific circumstance and after integrating twice, the differential equation can be reduced to one with discrete variables [using a new alteration of variables, $w(x) = y'(x)$]. As presented in Eq. (2). c and d are the constant values for two times integrations of Eq. (1).

$$\mathrm{EI}\frac{w'(x)}{\left(1+w^2(x)\right)^{3/2}} = cx + d \quad (2)$$

By integrating both sides of the aforementioned equation, the new equation can be presented as follows:

$$\mathrm{EI}\int\frac{w'(x)}{\left(1+w^2(x)\right)^{3/2}} = c\frac{x^2}{2} + dx + e \quad (3)$$

where from trigonometry rules,

$\cosh^2 a - \sinh^2 a = 1$

$w = t = \sinh^2 a$

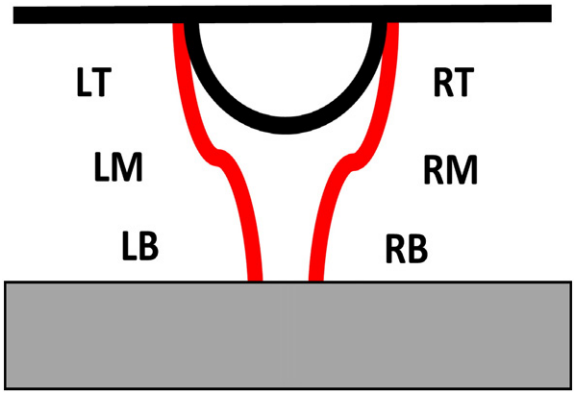

Fig. 10. Location of strain gauges in VSB half model. (a) model type 1, (b) model type 2, (c) model type 3, (d) model type 4.

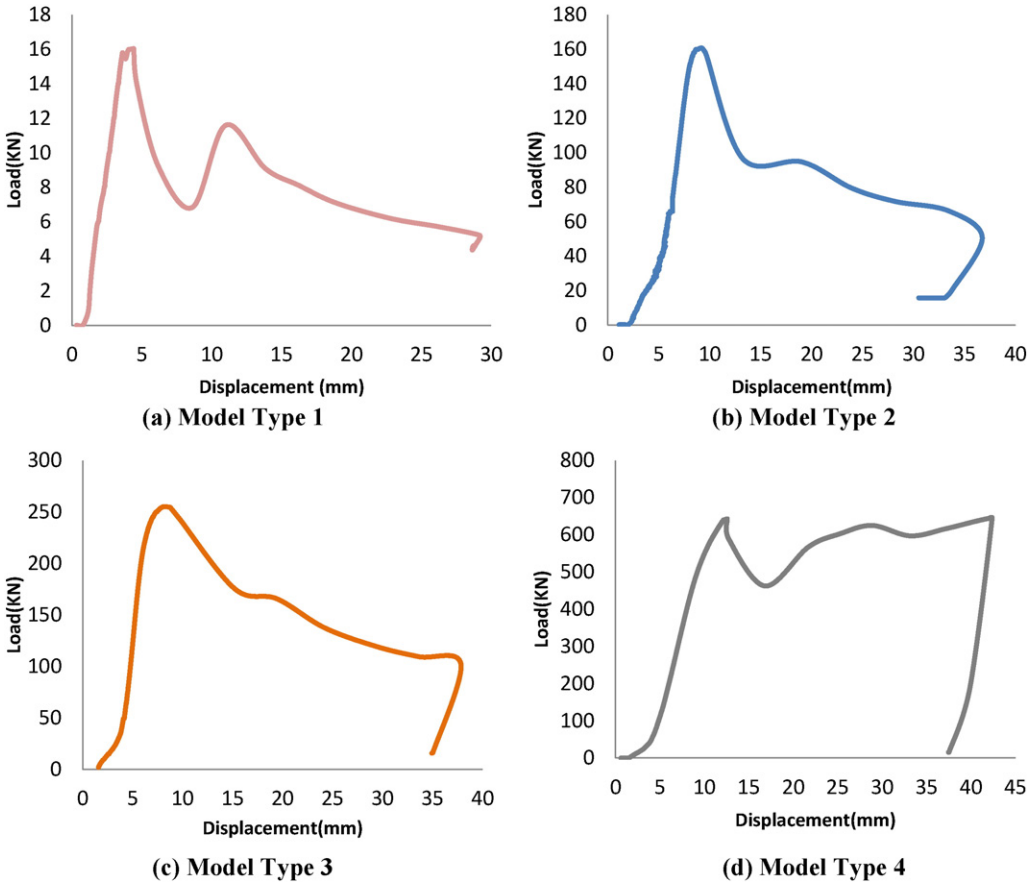

Fig. 11. Compression load vs. displacement graph of models. (a) Model type 1, (b) model type 2, (c) model type 3, (d) model type 4.

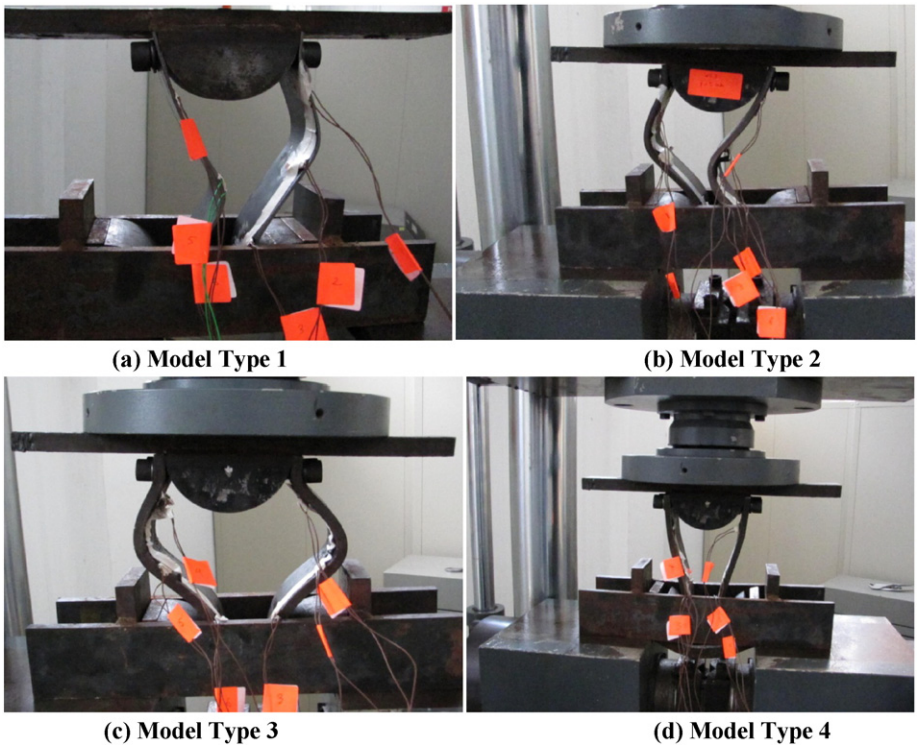

Fig. 12. Deformed shape of models after compression test. (a) Model type 1, (b) model type 2, (c) model type 3, (d) model type 4.

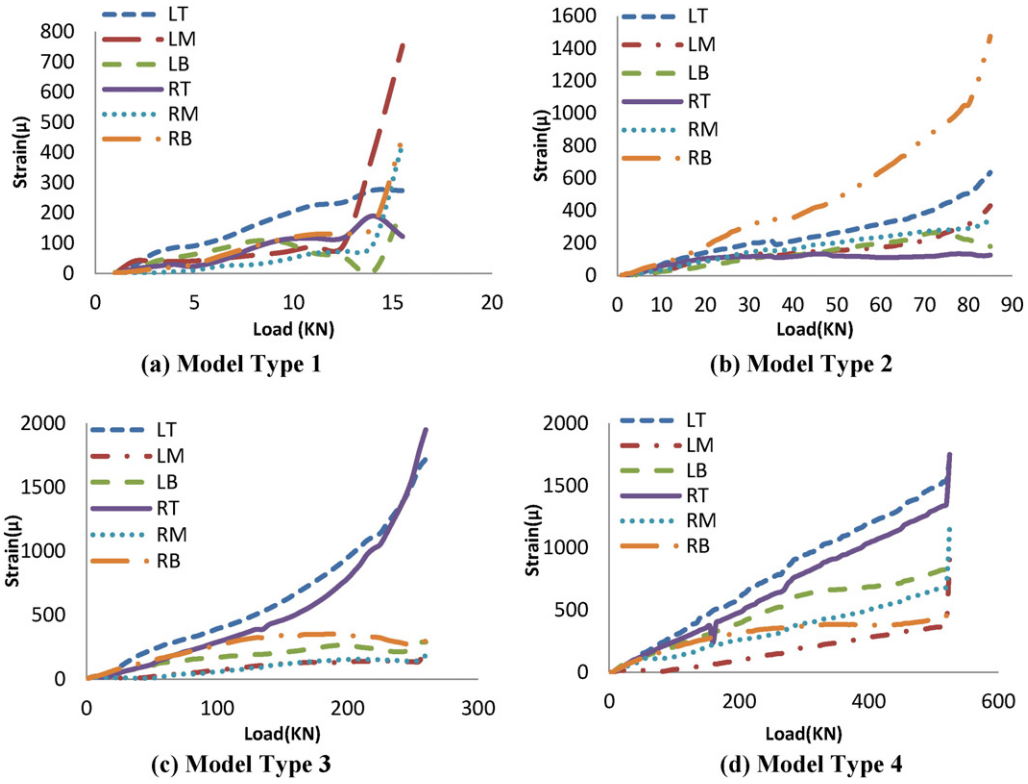

Fig. 13. Strain records of models.

where t is considered as variable.

$$dw = dt = \cosh^2 a\, da$$

The results of substitution of the above parameters in Eq. (3) can be expressed as follows:

$$\mathrm{EI}\int \frac{w'(x)}{(1+w^2(x))^{3/2}} = \mathrm{EI}\int \frac{\cosh a}{\cosh^3 a} da = \mathrm{EI}\tanh a = \frac{\mathrm{EI}t}{\sqrt{1+t^2}}$$

By applying the boundary conditions, the solution can be presented as

$$y\left(x_f^{\alpha}\right) = y_f + \int_0^{x_f^{\alpha}} \frac{\varphi\left(x^2 - x_f^{\alpha}.x\right)}{\sqrt{1-\varphi^2\left(x^2 - x_f^{\alpha}.x\right)^2}}\,\mathrm{dx}, \text{ for } 0 < x \le x_f^{\alpha} \tag{4}$$

where φ is an unknown variable that can be obtained from numerical integration by using the Gaussian points of Eq. (5). The value of (y^{a}_{f}) is equal to zero.

$$y\left(x_f^{\alpha}\right) = y_f + \int_0^{x_f^{\alpha}} \frac{\varphi\left(x^2 - x_f^{\alpha}.x\right)}{\sqrt{1-\varphi^2\left(x^2 - x_f^{\alpha}.x\right)^2}} dx = 0 \tag{5}$$

After using numerical Gaussian points and implementing the formula simplification based on normal mathematical sequences, the value of φ can be calculated using Eq. (4).

$$\varphi = \sqrt{\frac{36.01}{x_f^{\alpha 4}(\alpha^2+1)}} \tag{6}$$

4. Experimental setup of nonlinear curved spring under compression test

For the evaluation of the nonlinear action of the leaf spring, the direct compression test is conducted. Four models are tested with various thicknesses and material specifications. Three different spring plates with thicknesses of 2, 5, and 10 mm made of normal steel and a spring plate with a thickness of 10 mm made of abrasion-resistant steel (called AR500) are considered and named as Type 1, 2, 3, and 4, respectively. Fig. 8 shows the VSB half model for the direct compression test. Two leaf springs (Label 1) are clamped to the quarter cylindrical steel supports with a radius of 60 mm at the bottom part (Label 2) with four socket-head cap screws. The quarter supports are fastened to horizontal plates (Label 3) with four formed hex screws with a diameter of 14 mm. The upper sides of the curved spring are fastened to a half cylindrical steel component with a diameter of 120 mm (Label 4) by four socket-head cap screws with a diameter of 14 mm. The half cylindrical support is welded to an upper plate with a thickness of 20 mm. The base support consists of two 14 mm-thick vertical plates and one 20 mm-thick horizontal plate (Label 6). These plates are fully welded together with inner side plates (Label 3). To fix the model in the compression test setup, two holes are provided to lock the model to the compression test machine via socket-

Table 1
Material specifications in finite element simulation.

Material Type	ASTM A36	AR-500
Yield strength:	2.5 e + 008 N/m^2	12 e + 008 N/m^2
Tensile strength:	4 e + 008 N/m^2	15.5 e + 008 N/m^2
Elastic modulus:	2 e + 011 N/m^2	2.05 e + 011 N/m^2
Poisson's ratio:	0.26	0.26
Mass density:	7850 kg/m^3	7880 kg/m^3
Shear modulus:	7.93 e + 010 N/m^2	35.7 e + 010 N/m^2

head cap screw with a diameter of 20 mm. All the models are fabricated with the same height of 32 cm. Fig. 9 depicts the real prototype under the compression test setup.

Six strain gauges are attached to both curved leaf springs to observe the strain changes. The location of each strain gauge is the same in all the models. All strain gauges are labeled as shown in Fig. 10 and attached to the data logger. Therefore, strain values at different gauges are measured for each load increment. Gauges LT, LM, and LB are located at 6, 13, and 22 cm, respectively, from the top plate. Gauges RT, RM, and RB are located at positions symmetrical to Gauges LT, LM, and LB. Compression test at the top of the specimens was performed using Universal Testing Machine Zwick/Roell Amsler HB1000. In the specimens with 2 and 5 mm thickness of leaf spring, direct vertical compression loads applied in increments of 1 KN, but it changed to 5 KN for specimens with 10 mm thickness of spring fabricated with normal and abrasion-resistant steel. The rate of load application on each models were slow and equaled to 0.5 KN/s The direct vertical compression load transferred to the leaf spring in order t to evaluate the stiffness of the curved leaf springs.

4.1. Experimental results and discussion

The force versus displacement graphs of four models are presented in Fig. 11. As seen in Fig. 11(a), the maximum applied load on model type 1 (with a spring thickness of 2 mm) is only 16 KN at a displacement of 5 mm, whereas in model types 2, 3, and 4, the maximum values of compression load reach about 157, 254, and 645 KN, respectively, as shown in Fig. 11(b), (c), and (d). Furthermore, the corresponding displacements at maximum applied loads reach approximately 7, 8.5, and 11 mm for model types 2, 3, and 4, respectively. Therefore, based on model types 2 and 3, the maximum load increases about 10 times with an increase in the thickness of springs from 2 mm to 5 mm (2.5 times). In model type 3, the spring's thickness is 10 mm (around 5 and 2 times more than types 1 and type 2, respectively), but the failure capacity increases by about 16 and 1.6 times compared with model types 1 and 2, correspondingly.

Fig. 12 depicts the deformed shape of different models subjected to compression test. As shown in Fig. 12(a), whenever the compression load reaches the maximum value of 16 KN, the spring yields and plastic deformation occurs. Given the yielding of the spring, the overall capacity of the model decreases dramatically and drops to 6.82 KN at 8.6 mm, then it increases to 11.59 KN at 10.98 mm, and then declines again to 4.6 KN at 28.3 mm, at which point the test is stopped. Fig. 12(b) illustrates the plastic deformed shape of model type 2. This model can resist an applied compression load of up to 157 at 9.6 mm after which the spring yields. Given the large plastic deformation, the model cannot carry more compression load and it then slumps. The deformations in the aforementioned models do not happen in a symmetrical layout probably because of a slight eccentricity in the spring curve geometry from symmetrical axis. Fig. 12(c) and (d) present the deformed shape of model types 3 and 4, respectively. Model type 3 can sustain the maximum compression load of 254 KN at 9.7 mm, which is significantly decreased because the spring has yielded. In model type 4, however, the springs can resist the applied load of up to 645 KN, and plastic deformation does not occur in the springs. Based on Fig. 12(d), the horizontal bottom plate is bent because the welding collapses.

Fig. 13 shows the strain values recorded from different models at the same value of load steps. In model type 1 [see Fig. 13(a)], the maximum strain value is captured in the left spring near the upper bolt, whereas the value of strains in the right spring are quite smaller. Strain gauge LT located in the upper bolts of the left spring passes the yield strain at 6.5 KN. By contrast, in model type 2, as shown in Fig. 13(b), the maximum strain is reported in the right spring near the lower bolts, thereby indicating that the stress is not distributed equally in both springs probably because of the asymmetrical geometry of the curved springs, as previously mentioned, and definitely because the springs cannot deform in a symmetrical shape. Fig. 13(c) presents the strain record of model type 3. The strain distributions are the same to a particular extent and the maximum strain values are obtained near the upper bolts and exceed the yield strain at 55 KN. Strain record of model type 4 shows that the strain values for all channels (except LT and RT, which are located near the upper bolts) are smaller than the yielding strain of the abrasion-resistant steel (AR500),

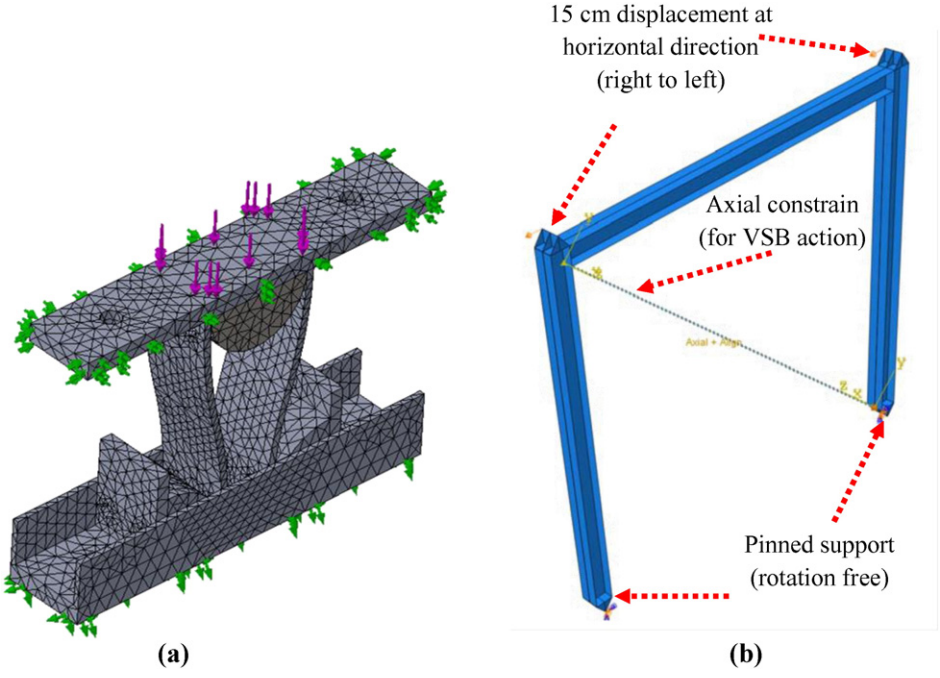

Fig. 14. (a) Mesh pattern of VSB half model and (b) one-bay steel frame model in ABAQUS. (a) Model type 1, (b) model type 2, (c) model type 3, (d) model type 4.

which is normally 10 times more than that of normal steel. Therefore, plastic deformation cannot be expected. From the record of model type 4, the stress patterns in the springs are the same because the strain distributions are approximately the same.

5. Procedure of finite element simulation

The same profile shape from the mathematical model has been inserted in the finite element simulation as presented previously in Fig. 7 and Eq. (4). All models used in the experiment are simulated in SOLIDWORKS Premium 2014 software. Static analysis is performed to evaluate the displacement value, which was compared with the experimental result under maximum load. Steel ASTM A36 is chosen as the springs' material for model types 1 to 3. In model type 4, the springs' material is Steel AR500 as presented in Table 1. The material for other components of the models is normal steel (ASTM A36). The bottom plate was used as the fixed boundary, and loads are applied as normal distributed force at gravity direction. Moreover, the movement of the top plate is adjusted to gravity direction. All components were meshed based on standard mesh. The meshes are curvature-based mesh with four Jacobin points. The springs and all components are high-quality solid elements. About 80.1% of the mesh's ratio is lower than 3. Fig. 14(a) demonstrates the mesh pattern of VSB half model. Given the mesh complexity and the compatibility issue of bolts in the models, all of them are excluded from analysis. Load values are based on the maximum value of the experimental results and the displacement of models are compared with those of the experimental specimens. To evaluate the efficiency of the VSB implementation in the frame, pushover analysis is conducted using the finite element simulation software ABAQUS version 6.11.1. The results from the experimental test of model type 2 are selected and applied in the bare steel frame with a height and width of 3 m. Beam and columns section are based on the profile of the universal column 152 × 152 × 30.15 cm. The force versus displacement values from the experimental test is used for the properties of the connector element located at a diagonal direction of the frame, as shown in Fig. 14(b). The frames' components are meshed as the shell element, and the normal material properties of structural steel are inputted in the software. Two one-bay steel frames are modeled with the same geometry specifications, material properties, and boundary conditions with and without diagonal axial connector element. Both models are constrained at their bases with pinned supports. In addition, both frames are subjected to 15 cm horizontal displacement to obtain the

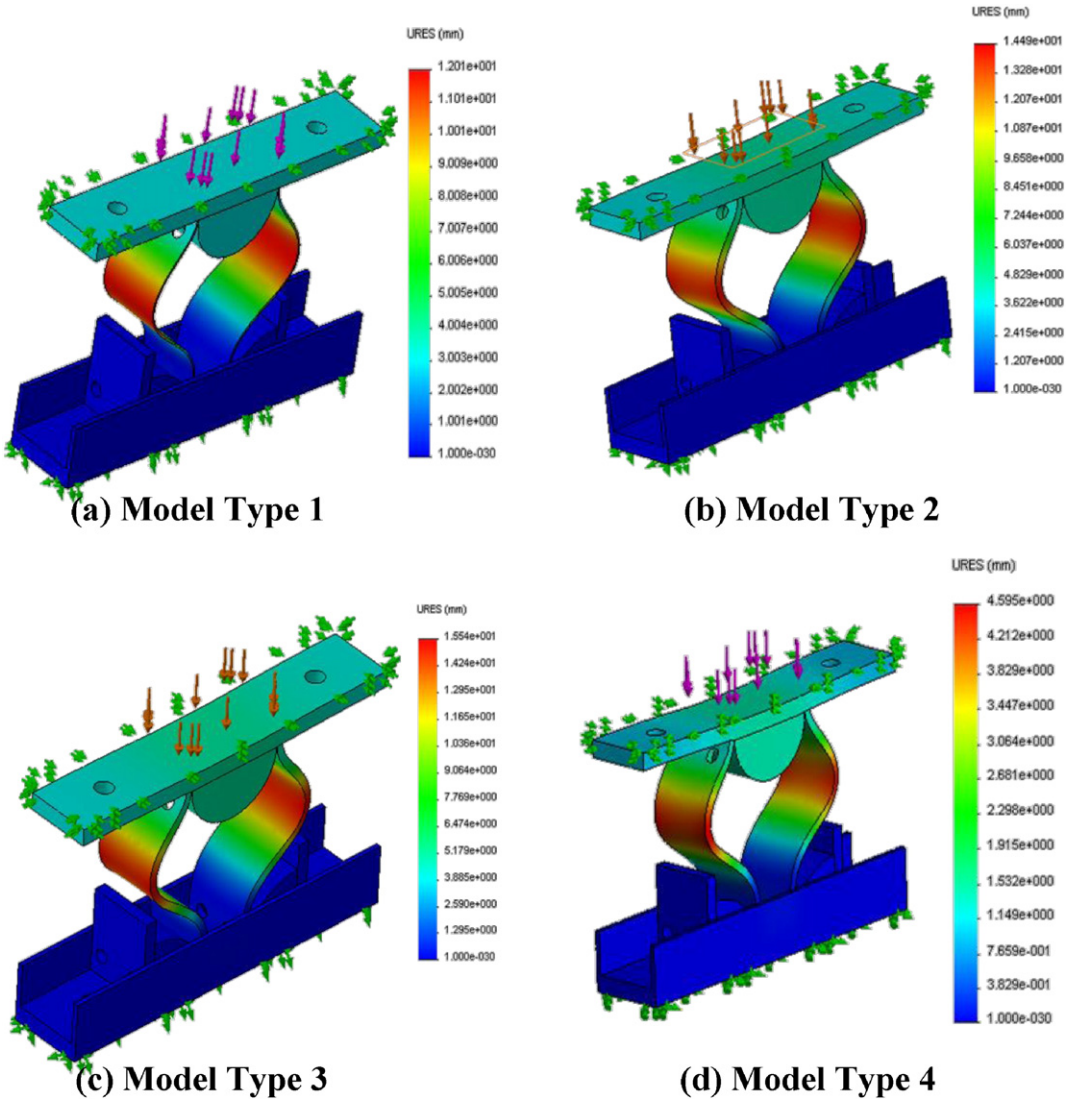

Fig. 15. Displacement reaction of the models. (a) Model type 1, (b) model type 2 (c) model type 3, (d) model type 4.

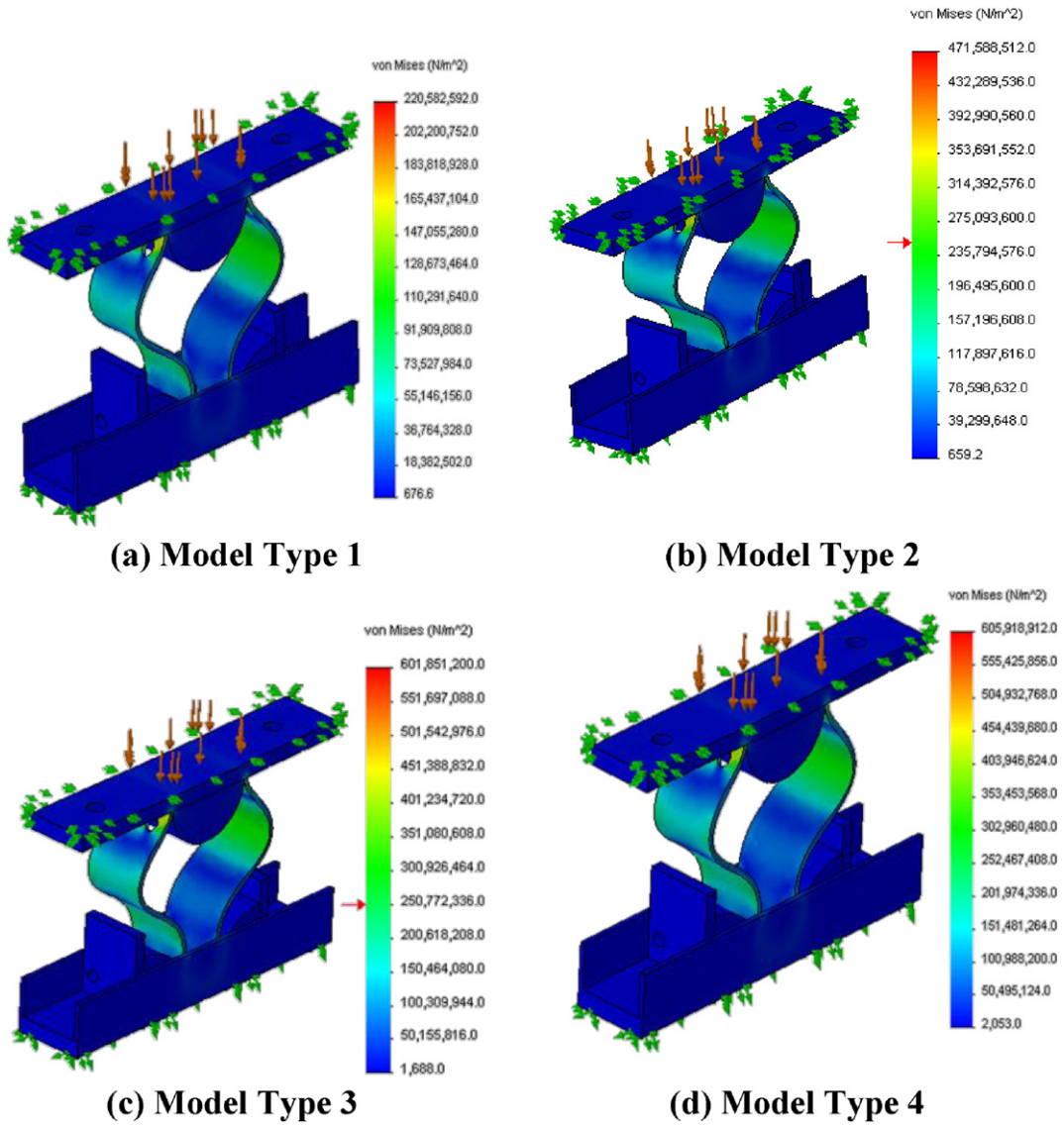

Fig. 16. Stress distribution of the models.

displacement versus base shear graph. The VSB device's function is considered as an axial element which constrained the extension movement of corner nodes, based on implemented force-displacement relation obtained from experimental test. The 15 cm displacement applied from right to left to plot shear-displacement (Pushover) graphs, for simplification the axial constrain implemented in one side only. The configuration for damper which described and presented in Fig. (2) is for structure subjected to cyclic or earthquake load which vibration occurred in both directions. For this reason design and all parts of damper device are symmetric to make functioning of device for both directions during vibration. The push over analysis is conducted to evaluate the behavior of device where subjected to the lateral displacement push in one direction of movement only. Therefore one side of device is functioning and for simplifying of modeling just half part of device is considered as implemented in bracing.

5.1. Simulation results

All model types are simulated at the maximum values of applied force obtained from the experiments. The results are evaluated in terms of displacement in the model and stress patterns. As shown in Fig. 15 the results reveal that the maximum displacements of model types 1, 2, 3, and 4 are roughly around 12, 14.5, 15.5, and 4.6 mm, respectively, which are higher than their corresponding displacements from the experimental tests. The stress patterns of each model at the applied load are presented in Fig. 16. In model type 1, the maximum stress is

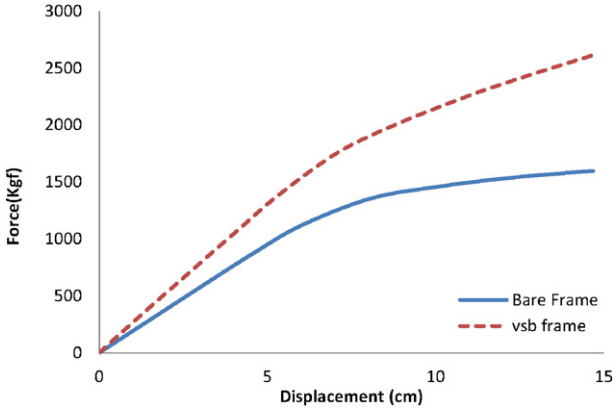

Fig. 17. Pushover curves for one-bay steel frames with and without VSB system.

Table 2
Compassion of maximum recorded displacement at top plates.

Model's type	Max displacement from test (mm)	Max displacement from FE simulation (mm)	Differences (%)
1	5.01	4.00	25
2	9.1	4.83	47
3	8.28	5.18	37
4	12.59	1.53	87

1568 MPa and is concentrated around the holes where the springs are fastened to the upper supports. When the yielding stress for normal steel is 250 MPa, the leaf springs in model types 1, 2, and 3 yield, as observed in the experimental results. In model type 4, the yield stress is 1200 MPa, which is about 4.5 times more than normal steel's yielding stress. As presented in Fig. 16(d) the springs do not yield except around the upper holes and a small portion of springs, as also detected in the experimental test.

In addition, the results from the implementation of the VSB system in the one-bay steel frame is reported in terms of pushover capacity curve in bare frame and VSB frame. As shown in Fig. 17, the maximum capacity of the frame equipped with VSB system increases by approximately 65% compared to that of bare frame. Therefore, the implementation of the VSB system in the frame enhances the failure capacity of the structure as well as increases the ductility of the structure.

6. Comparison between FE and experimental results

Since the finite element simulation and experimental test were conducted in this study, the comparisons between them are reported in terms of maximum displacement at top plate and maximum stress at the middle of spring where the strain gauges are located. The summary on mentioned comparison is recorded in Tables 2 and 3. In model type 1, 2 and 3 the differences of maximum displacement at top plate from experiments and finite element simulation are reported 25, 47 and 37% respectively. At model type 4, the maximum displacement of top plate was affected by bending of horizontal base plate due to insufficient strength of welding. Therefore the differences between test and simulation are reached to 87%. Since in the simulation the horizontal and vertical base plates are bounded act together the bending of base plate was not observed which resulted in enormous difference. Furthermore Figs. 18 and 19 present the maximum displacement and stress obtain from experimental test and finite element simulation.

7. Conclusion and recommendation

In this research, a VSB system that is applicable to a framed building is proposed. The VSB system can be added as supplementary device to absorb the vibration energy induce by earthquake, wind and etc. and mitigate the damage from main structural component. A mathematical modeling is performed to obtain the shape profile of the curved spring,

Table 3
Compassion of stress value at the mid of spring.

Model's type	Max stress from test (MPa)	Max stress from FE simulation (MPa)	Differences (%)
1	150,800,000	147,055,280	2.54
2	295,000,000	314,392,576	6.17
3	356,400,000	401,234,720	11.17
4	350,000,000	403,946,624	13.35

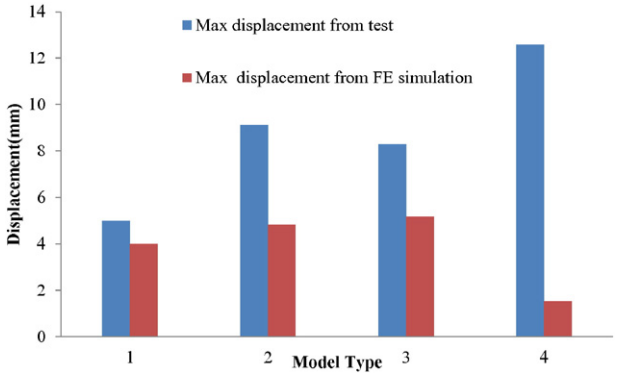

Fig. 18. Maximum displacement from FE simulation and experimental test.

which is the most important component of the VSB system. Direct compression experiments are also conducted on four models with different thicknesses and material specifications. Moreover, the VSB half models are simulated to assess and compare the spring behavior at the same maximum value of force obtained from the experiments. The results from both the simulation and experiments have good agreement in terms of VSB behavior at the applied load. Furthermore, the efficiency of VSB implementation in the structure is evaluated based on pushover analysis in one-bay steel frame, and the results reveal the high competence of VSB application in the frame as a lateral resistance system. Further studies must be conducted in different aspects, including optimization of proposed system, parametric analysis of VSB system, and experimental test of the frame model. Variable stiffness bracing system has shown enough capability to put into practice as a cheap and simple product to install in new and existing framed buildings to reduced and eliminate the structural damage due to the earthquake. Fabrication price is around 500 USD which is about 6% to 10% of available dampers 'devices' in market.

Acknowledgements

This work received financial support from the Ministry of Science, Technology and Innovation, Malaysia under research project no. 5524254 and was further supported by the University Putra Malaysia under Putra grant No. 9415100. This support is gratefully acknowledged. Moreover, the variable stiffness bracing system has

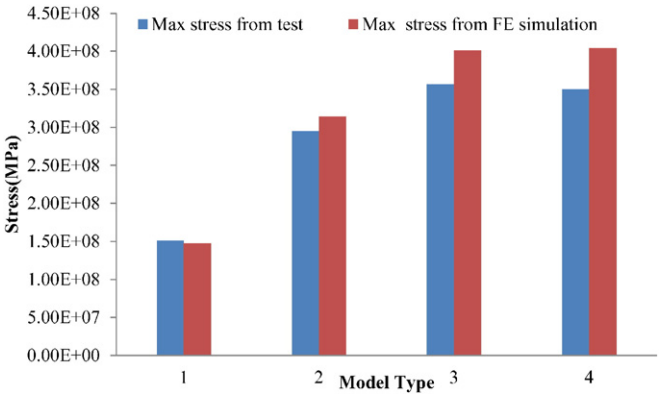

Fig. 19. Maximum stress from FE simulation and experimental test.

been filed for patent grant at Malaysian Intellectual Property Organization (MyIPO) under application no. PI 2014701608.

References

[1] B.F. Spencer Jr., S. Nagarajaiah, State of the art of structural control, J. Struct. Eng. 129 (7) (2003) 845–856.
[2] T. Soong, G. Dargush, Passive Energy Dissipation Systems in Structural Engineering, John Wiley & Sons, New York, NY, 1997.
[3] M.D. Symans, F.A. Charney, A.S. Whittaker, M.C. Constantinou, C.A. Kircher, M.W. Johnson, et al., Energy dissipation systems for seismic applications: current practice and recent developments, J. Struct. Eng. 134 (1) (2008) 3–21.
[4] J.T. Yao, Concept of structural control, J. Struct. Div. 98 (7) (1972) 1567–1574.
[5] M.J. Crosby, R.A. Harwood, D. Karnopp, Vibration Control Using Semi-Active Force Generators, Transactions of the ASME, Paper, 1974.
[6] T. Kobori, M. Takahashi, T. Nasu, N. Niwa, K. Ogasawara, Seismic response controlled structure with active variable stiffness system, Earthq. Eng. Struct. Dyn. 22 (11) (1993) 925–941.
[7] J.N. Yang, J.C. Wu, Z. Li, Control of seismic-excited buildings using active variable stiffness systems, Eng. Struct. 18 (8) (1996) 589–596.
[8] K. Yamada, T. Kobori, Control algorithm for estimating future responses of active variable stiffness structure, Earthq. Eng. Struct. Dyn. 24 (8) (1995) 1085–1099.
[9] S. Kamagata, T. Kobori, Autonomous Adaptive Control of Active Variable Stiffness System for Seismic Ground Motion“Proc., First World Com”. on Struct. Control 4 (1994) 33–42.
[10] T. Kobori, S. Kamagata, Dynamic intelligent buildings—active seismic response control, Intell. Struct. 2 (1992) 279-274.
[11] T. Nasu, T. Kobori, M. Takahashi, N. Niwa, K. Ogasawara, Active variable stiffness system with non-resonant control, Earthq. Eng. Struct. Dyn. 30 (11) (2001) 1597–1614.
[12] M. Azadi, S. Behzadipour, G. Faulkner, Performance analysis of a semi-active mount made by a new variable stiffness spring, J. Sound Vib. 330 (12) (2011) 2733–2746.
[13] A.G. Rodriguez, N.E.N. Rodriguez, A.G.G. Rodriguez, Design and validation of novel actuator with adaptable compliance for application in human-like robotics, Ind. Robot. 36 (1) (2009) 84–90.
[14] F. Hejazi, J. Noorzaei, M.S. Jaafar, W.A. Thanoon, A. AAA, Optimization of active variable stiffness system for controlling structural response of a building under earthquake excitation, J. Struct. Eng. 36 (4) (2009) 235–242.
[15] F. Hejazi, I. Toloue, M.S. Jaafar, J. Noorzaei, Optimization of earthquake energy dissipation system by genetic algorithm, Comput.-Aided Civ. Infrastruct. Eng. 28 (10) (2013) 796–810.
[16] L.C. Visser, R. Carloni, R. Unal, S. Stramigioli, Modeling and design of energy efficient variable stiffness actuators, in robotics and automation (ICRA), IEEE Int. Conf. 2010 (2010) 3273–3278.
[17] D.C. Nemir, Y. Lin, R.A. Osegueda, Semiactive motion control using variable stiffness, J. Struct. Eng. 120 (4) (1994) 1291–1306.
[18] S. Nagarajaiah, E. Sonmez, Structures with semiactive variable stiffness single/multiple tuned mass dampers, J. Struct. Eng. 133 (1) (2007) 67–77.
[19] M.D. Symans, M.C. Constantinou, Semi-active control systems for seismic protection of structures: a state-of-the-art review, Eng. Struct. 21 (6) (1999) 469–487.
[20] B. Wu, Seismic design method of structures with active variable stiffness systems, J. Vib. Eng. 2 (1990) (2002) 1009–1016.
[21] S. Nagarajaiah, N. Varadarajan, Novel semi-active variable stiffness tuned mass damper with real time tuning capability, Proceeding of 13th Engineering Mechanics Conference, 2000.
[22] J. Kang, H. Kim, D. Lee, Mitigation of wind response of a tall building using semi-active tuned mass dampers, Struct. Des. Tall Spec. Build. 20 (5) (2011) 552–565.
[23] N. Varadarajan, S. Nagarajaiah, Response Control of Building with Variable Stiffness Tuned Mass Damper Using Empirical Mode Decomposition and Hilbert Transform Algorithm, 16th ASCE Engineering Mechanics Conference, 2003.
[24] O. El-Khoury, H. Adeli, Recent advances on vibration control of structures under dynamic loading, Arch. Comput. Meth. Eng. 20 (4) (2013) 353–360.
[25] L.Y. Lu, S.Y. Chu, S.W. Yeh, L.L. Chung, Seismic test of least-input-energy control with ground velocity feedback for variable-stiffness isolation systems, J. Sound Vib. 331 (4) (2012) 767–784.
[26] M. Bruneau, C.M. Uang, A. Whittaker, Ductile Design of Steel Structures, McGraw-Hill, New York, 1998.
[27] A. Fateh, F. Hejazi, M.S. Jaafar, A. Adnan, Dynamic analysis of variable stiffness bracing system in structure, Appl. Mech. Mater. 704 (2015) 442–446.
[28] R. Frich-Fay, Flexible Bars, Butterworths, Washington, 1962.